HHS Public Access

Author manuscript

Cell Stem Cell. Author manuscript; available in PMC 2017 January 07.

Published in final edited form as:

Cell Stem Cell. 2016 January 7; 18(1): 134–143. doi:10.1016/j.stem.2015.10.002.

Functional connectivity under optogenetic control allows modeling of human neuromuscular disease

Julius A. Steinbeck[1,2], **Manoj K. Jaiswal**[3], **Elizabeth L Calder**[1,2], **Sarah Kishinevsky**[1,2], **Andreas Weishaupt**[5], **Klaus V. Toyka**[5], **Peter A. Goldstein**[3,4], and **Lorenz Studer**[1,2,*]

[1]The Center for Stem Cell Biology, Sloan-Kettering Institute for Cancer Research, New York, NY 10065, USA

[2]Developmental Biology Program, Sloan-Kettering Institute for Cancer Research, New York, NY 10065, USA

[3]Department of Anesthesiology, Weill Cornell Medical College, New York, NY 10065, USA

[4]Department of Medicine, Weill Cornell Medical College, New York, NY 10065, USA

[5]Department of Neurology, University of Wuerzburg, 97080 Wuerzburg, Germany

Summary

Capturing the full potential of human pluripotent stem cell (PSC)-derived neurons in disease modeling and regenerative medicine requires analysis in complex functional systems. Here we establish optogenetic control in human PSC-derived spinal motorneurons and show that co-culture of these cells with human myoblast-derived skeletal muscle builds a functional all-human neuromuscular junction that can be triggered to twitch upon light stimulation. To model neuromuscular disease we incubated these co-cultures with IgG from myasthenia gravis patients and active complement. Myasthenia gravis is an autoimmune disorder that selectively targets neuromuscular junctions. We saw a reversible reduction in the amplitude of muscle contractions, representing a surrogate marker for the characteristic loss of muscle strength seen in this disease. The ability to recapitulate key aspects of disease pathology and its symptomatic treatment suggests that this neuromuscular junction assay has significant potential for modeling of neuromuscular disease and regeneration.

*Corresponding authors: Lorenz Studer: studerl@mskcc.org; Julius Steinbeck: just.msk@use.startmail.com.

AUTHOR CONTRIBUTIONS

J.A.S.: Conception and study design, hESC manipulation, differentiation and characterization, co-culture assays, calcium imaging, immunohistochemistry, qPCR experiments data analysis and interpretation and writing of manuscript. M.K.J.: Study design, electrophysiological experiments, data analysis and interpretation. E.L.C.: Development of the MN protocol, qPCR experiments, data analysis and interpretation. S.K.: LDH toxicity assay, data analysis and interpretation. A.W.: Provision of materials. K.V.T.: Study design, provision of materials, data interpretation. P.A.G.: Study design, data analysis and interpretation, writing of manuscript. L.S.: Conception and study design, data analysis and interpretation, writing of manuscript.

INTRODUCTION

Application of PSC-derived neurons in regenerative medicine and disease modeling ideally requires their integration into complex functional human networks or tissues. For several CNS cell types this need has been addressed by the development of more integrative tissue engineering approaches where pluripotent cells were used to generate miniature three-dimensional model versions of human organs (Lancaster and Knoblich, 2014). Yet, one of the most important properties of neurons, namely their ability to form functional synapses and transmit information to appropriate downstream targets, remains largely unexplored in human organoids and other PSC-based model systems. Recent studies have started to integrate optogenetics, a technique that allows for light-mediated, millisecond-precise activation of genetically targeted neuronal populations (Boyden et al., 2005; Zhang et al., 2011), into PSC-based regenerative medicine paradigms (Bryson et al., 2014; Cunningham et al., 2014; Steinbeck et al., 2015). We therefore hypothesized that optogenetics may similarly enable the assessment of neuronal connectivity in an all-human complex culture system such as a neuromuscular co-culture.

Remarkable progress has been made in the generation of spinal motorneurons from human PSCs (Amoroso et al., 2013; Calder et al., 2015; Chan et al., 2007; Davis-Dusenbery et al., 2014; Maury et al., 2015) but their ability to functionally connect to and control human skeletal muscle function has not been assessed. The connection between spinal motorneurons and skeletal muscle is the crucial final pathway of the human pyramidal motor system controlling voluntary movements (Barker et al., 1985). It is severely affected in many traumatic, degenerative and inflammatory diseases, which are classically believed to affect mainly either the neuronal (Kuwabara and Yuki, 2013; Sendtner, 2014; Silva et al., 2014; Titulaer et al., 2011), or the muscle side (Mercuri and Muntoni, 2013; Plomp et al., 2015) of the neuromuscular junction. It is clear that muscle denervation and re-innervation dramatically alter muscle physiology (Cisterna et al., 2014; Daube and Rubin, 2009). Vice versa, there is increasing evidence that muscle-dependent trophic, cell adhesion, and axon-guidance signals play an essential role in the formation and maintenance of the neuromuscular junction. Physiological activity such as exercise or pathological conditions such as ALS and other neuromuscular disorders greatly affect strength and function of the neuromuscular junction (Moloney et al., 2014). Similar to an animal model, a human system to study neuromuscular development and disease should comprise of the main components of the neuromuscular junction including spinal motorneurons and skeletal muscle and be amenable to functional testing and manipulation.

RESULTS

Optogenetic control in human spinal motorneurons

To establish optogenetic control in a human spinal MN population we transduced undifferentiated H9 hESCs with lentiviral vectors for the expression of Channelrhodopsin2-EYFP or EYFP alone under control of the human synapsin promoter. The synapsin promoter was selected for its faithful and robust expression in human PSC-derived neurons. Clonal hESC lines were expanded and validated by PCR for genomic integration of the transgenes (data not shown) as well as maintenance of pluripotency marker expression (Figure 1A, O).

Only ESC clones with robust transgene expression across various neuronal differentiation paradigms (Steinbeck et al., 2015) were selected for further experiments. Differentiation into spinal motorneurons was achieved by combining dual SMAD inhibition (Chambers et al., 2009) with activation of the hedgehog pathway for ventralization and exposure to retinoic acid for caudalization (Calder et al., 2015). By day 20 of differentiation the ChR2-EYFP transgene was expressed strongly in the neuronal clusters emerging under those culture conditions (Figure 1B). We developed a simple purification procedure involving dissociation of the cultures on day 20 and sedimentation of the neuronal clusters while the supernatant, containing the non-neuronal cells, was discarded. This strategy allowed for a significant purification of hESC-derived MNs (Figure 1C). qRT-PCR analysis of 5 consecutive MN differentiations confirmed a 3-fold enrichment of the bona-fide sMN markers ISL1, NKX6.1 and OLIG2 in purified MN cultures (Figure 1D), whereas markers for non-neuronal contaminants (FOXA2, PDX1) were approximately 10-fold depleted in purified MN cultures (Figure 1E). In an additional qRT-PCR experiment on purified MNs on day 40 we found the physiologically relevant MN markers choline acetyltransferase (ChAT) acetylcholine esterase (ACHE) and agrin (AG) to be expressed (CHAT 60.3 ± 29.6 % of HPRT, ACHE 273.6 ± 59.3 % of HPRT, AG 79.3 ± 32.1% of HPRT). By immunocytochemistry we confirmed that purified MNs expressed HB9 and ISL1 in combination with ChR2-EYFP (Figure 1F) as well as ChAT and the mature neurofilament marker SMI32 (Figure 1G). An alternative protocol for MN induction (Maury et al., 2015) produced comparable results (Figure 1H–J). Optogenetic control was validated in electrophysiological experiments. In matured spinal motorneurons (beyond day 60), which were identified under bright field and green fluorescent optics (Figure 1K), resting membrane potential was −62.4 ± 4.8 mV (SEM). Tonic action potential (AP) firing was evoked from a membrane potential held at −70 ± 2 mV by injection of depolarizing current steps (Figure 1L). In addition, 4 out of 4 ChR2 expressing neurons fired light-induced APs over a broad frequency range form 0.2 – 10 Hz (Figure 1M, N). Spike fidelity was 100% from 0.2 to 2 Hz, 93.3 ± 5.7 % at 5 Hz and 65.5 ± 23.3 % at 10 Hz. Purified neurons from the EYFP hESC line also expressed HB9 and ISL1 (Figure 1 O, P). Resting membrane potential was −58.4 ± 2.6 mV (SEM). These control neurons could be induced to fire APs by current injection (Figure 1Q). But as expected, 2 out of 2 tested EYFP+ neurons did not respond to any light stimulation (Figure 1R).

Functional human skeletal muscle

To obtain functional skeletal muscle in vitro, we used human primary myoblasts from an adult (hMA) and a fetal donor (hMF). Both types of myoblasts (Figure 2A) were induced to differentiate when they reached 70% confluence. Both myoblast cultures fused to form multinucleated myotubes within 4 to 7 days after the initiation of differentiation. Stimulation with acetylcholine (ACh, 50μM) caused adult and fetal myofibers to contract with increasing reliability from day 10 to day 17 (Figure 2B and S1A, B). Muscle functionality was further assessed in calcium imaging experiments. Muscle cultures plated on glass coverslips were incubated with the calcium dye Fura2 on day 35 of differentiation. After stimulation with ACh the fibers generated a distinct calcium transient (Figure 2C and S1C, D). Quantification of AChR subunits by qRT-PCR revealed that day 30 muscle cultures expressed the fetal gamma subunit (CHRNG, 32.2 ± 8.6% of HPRT in hMA cultures and 97.1 ± 33.4 % of

HPRT in hMF cultures) whereas the adult epsilon subunit was almost undetectable (CHRNE < 0.2% of HPRT expression in hMA and hMF cultures, CHRNG:CHRNE ratio > 100 for both muscle types). Human myo-cultures also expressed muscle specific kinase (MuSK, 44.8 ± 18.5% of HPRT in hMA cultures and 73.8 ± 15.8 % of HPRT in hMF cultures). Immunocytochemical analysis confirmed that multinucleated myotubes expressed fast skeletal muscle myosin (Fig S1E), whereas the mesenchymal stroma expressed the intermediate filament vimentin (Fig S1F). Structurally intact myotubes could be maintained in culture at least until day 90, but did not develop the typical skeletal muscle striation under these conditions in the absence of motorneurons (Figure S1G, H).

Generation of functional human neuromuscular co-cultures

To establish the neuromuscular co-culture, we used the purified ChR2-expressing spinal motorneurons (day 20–25) and plated them onto pre-differentiated skeletal myofibers (day 5–10). After plating, hESC-derived spinal MN cell bodies mostly remained within the neuronal clusters but extended axons across the adult and fetal muscle (up to 2 mm within the first week, Figure 3A, E). Co-cultures were tested for the establishment of neuromuscular connectivity in weekly intervals. For this purpose the cultures were observed under bright field illumination and intermittently stimulated with blue light pulses. Six to eight weeks after initiation of the co-culture, the elongated cylindrical myoblast-derived muscle fibers remained morphologically intact and started to contract in response optogenetic stimulation (470 nm, 0.2 Hz, 300 ms pulse width). Figures / Videos 3B, F show mature co-cultures with both muscle types. Figure 3C, G show the quantification of muscle twitches of individual fibers from such cultures (for videos see Figure S2B, C, H, I). The lower panels of Fig. 3C, G show extended stimulation over 500 seconds (Fig 3C at 0.2 Hz, Fig 3G at 0.1 Hz). 630 nm light never caused any muscle contraction (Figure S2D), indicating that muscle twitching was a result of ChR2 activation. Addition of vecuronium (2μM), an antagonist of the nicotinic acetylcholine receptor (AChR) completely blocked the light induced muscle twitches in all tested cultures (Figure 3D, H and videos Figure S2 E, L). These data indicate that connectivity was indeed established through a functional neuromuscular cholinergic synapse and not the result of cell fusion (i.e. ChR2 transfer into the muscle membrane which would cause direct muscle activation). Similar results were achieved when ChR2+ MNs generated through the alternative protocol (Maury et al., 2015) were plated onto hMA- (Figure S2 J, K, L) or hMF-derived muscle (data not shown). Most MN-only cultures never showed any light induced twitching (Figure S3A–C). However, approximately 20% of long-term MN-only cultures produced a non-neural overgrowth, which sometimes displayed light induced, vecuronium sensitive twitching (Figure S3D–G). These data suggest that MN cultures with suboptimal purification may contain PSC-derived myogenic cells. Alternatively, the derivation of precursors capable of generating both spinal motorneurons and paraxial mesodermal structures including skeletal muscle has been reported recently (Gouti et al., 2014). However, such PSC-derived muscle-like cells never showed the isolated, elongated morphology typical for primary myoblast-derived fibers,

We next characterized key physiologic parameters in the functional neuromuscular cultures. Matured co-cultures were incubated with the calcium dye Fura2 and mounted into an imaging chamber for continuous perfusion. In regions that were previously identified to

show muscle contraction in response to light stimulation (Figure 3I), 470 nm optogenetic stimulation produced calcium spikes in myofibers, which could be blocked by vecuronium (6 out of 6 cultures, Figure 3J). The lower panel of Figure 3J confirms stability of neuromuscular excitability in a calcium imaging experiment over 45 minutes (n=3). In a separate study, skeletal myotubes (n=5), identified by their cylindrical and striated appearance under phase contrast microscopy and by their ability to undergo light-induced twitching were selected for intracellular recordings (Figure 3K). Light-responsive myotubes were impaled with sharp microelectrodes and muscle APs were recorded during 447 nm optogenetic stimulation at frequencies from 0.2 to 2 Hz. Spike fidelity was 100% at 0.2 Hz, 93.3 ± 6.7 % at 0.5 Hz, 75 ± 15.0 % at 1 Hz and 80 ± 10.0 % at 2 Hz. Vecuronium (2μM) completely blocked light-induced APs in myofibers in a reversible manner. To address the long-term stability of neuromuscular connectivity over the course of several days and weeks, contractile regions (n=7) were assessed every 5 days. Quantitative analysis revealed that all 7 regions remained responsive to optogenetic stimulation and contraction increased to 137.3 ± 50.7% until day 25 as compared to day 0 (Fig. 3L).

Morphological characterization revealed the presence of a layer of non-neuronal cells, potentially representing stromal cells that may be necessary to hold the contracting muscle in place. The majority of these stromal cells expressed vimentin and a minority GFAP (Fig. 1M). In most contractile regions a dense network of neuronal processes was found in close contact with myotubes staining for desmin (Figure 3N) or myosin (data not shown). Neuronal EYFP+ boutons were found to be in close contact with striated, multinucleated muscle fibers (Figure 3O). The acetylcholine receptor located on myofibers was labeled with bungarotoxin (BTX). High power confocal imaging (Figure 3P and S2M) revealed plaque-like clustering (Marques et al., 2000) of the acetylcholine receptor on muscle membranes in close apposition to MN synaptic terminals. Quantification of BTX+ dots on myofibers revealed a significant increase in contracting and strongly innervated regions as compared to non-contracting regions (Fig 3Q, R; two-tailed unpaired t test, $p = 0.016$, $t = 2.60$). Quantification of AChR subunits by qRT-PCR revealed that co-cultures matured for 6 weeks expressed the fetal gamma subunit (CHRNG, 17.3 ± 7.5% of HPRT in hMA co-cultures and 27.4 ± 9.0 % of HPRT in hMF co-cultures) whereas the adult epsilon subunit was almost undetectable (CHRNE < 0.1% of HPRT expression in hMA and hMF co-cultures, CHRNG:CHRNE ratio > 100 for both co-culture types). Therefore, co-culturing with human spinal motorneurons did not induce expression of the adult epsilon subunit within the time frame studied here. Neuromuscular co-cultures also expressed muscle specific kinase (MuSK, 7.9 ± 1.9% of HPRT in hMA co-cultures and 27.7 ± 10.3 % of HPRT in hMF co-cultures).

Myasthenia gravis disease modeling

Next we sought to address whether the functional neuromuscular co-cultures were suitable to model a classic human neuromuscular disease. Myasthenia gravis (MG) (Toyka et al., 1977; Verschuuren et al., 2013) is caused by the emergence of autoantibodies against proteins in the neuromuscular junction (e.g. the acetylcholine receptor, AChR). Binding of the pathogenic antibody to AChR activates the complement cascade, resulting in destruction of the neuromuscular endplate (Sahashi et al., 1980), which ultimately causes progressive

muscle weakness in patients. We therefore quantified light-induced muscle contractions in functional co-cultures of MNs with adult-derived myoblasts (hMA) before (Figure 4A, D and Figure S4A, D, G) and after the incubation with purified IgG fractions (200 nM total IgG) from two MG patients with clearly elevated AChR antibody titers (#1 and #2). Sandoglobulin (SG) polyvalent IgG served as control. Fresh human serum (2%) containing active complement was added together with all IgGs. When the exact same culture regions were tested again three days after IgG and complement exposure, we found that muscle twitches in response to light stimulation were reduced in cultures incubated with MG IgG and complement (Figure 4B and S4B, E) but not in control cultures incubated with control IgG and complement (Figure 4E, S4H). Quantification of muscle twitches in contractile cultures revealed that compared to the initial movement before addition of IgG and complement (day 0, 100%) control cultures showed an increase in muscle contraction to 125% on day 3 (n=14). In contrast, cultures incubated with IgG from either of the MG patients showed a significant decrease (MG#1, 68% n=14, and MG#2, 60%, n=11) in contractility (Figure 4G, One-way ANOVA, $p = 0.0046$, $F(2,36) = 6.25$). Dunnett's multiple comparisons test revealed significant differences between the control group and either of the MG groups (CTRL vs. MG#1, $p < 0.05$, $q = 2.93$ and CTRL vs. MG#2, $p < 0.01$, $q = 3.13$), suggesting that a myasthenic phenotype had been introduced. To test if treatment responses could be modulated as in the human disease, we incubated MG cultures (Figure 4C and S4C, F, n=8) and controls (Figure 4F and S4I, n=4) with the ACh esterase inhibitor pyridostigmine (PYR, 10 μM). We found that PYR application in MG cultures induced a significant therapeutic effect (Figure 4C and 4H, +22%, two-tailed paired t test, $p = 0.002$, $t = 4.69$). Next, we assessed if the myasthenic phenotype was reversible after washout of MG IgG and complement, mimicking plasmapheresis therapy (Gold et al., 2008). MG IgG and complement were added to the media on day 0 and identical culture regions (n=4) were tested again 1 and 3 days after wash out on day 3 (days 4 and 6, respectively). Quantitative analyses revealed that in 4 out of 4 cultures, wash out of MG IgG and complement resulted in the reversal of the myasthenic phenotype (Figure 4I, D3 vs. D6, two-tailed paired t test, $p = 0.0098$, $t = 10.09$). We also tested the effect of control and MG#1 IgG without the addition of complement over a 7-day time course. Untreated cultures (n=5) and cultures treated with CTRL IgG (n=6) increased in contractility over time, whereas cultures treated with MG#1 IgG (n=7) showed a delayed but significant decrease in contractility to approximately 70% on day 5 and day 7 (CTRL vs. MG on day 7, Dunnett's multiple comparisons test, $p < 0.05$, $q = 3.10$). This complement-independent effect may be attributed to AChR crosslinking by the pathogenic antibody (Drachman et al., 1978).

To further characterize the myasthenic phenotype we performed calcium imaging experiments. Acute application of MG#1 IgG did not reduce the light induced calcium signal recorded from myofibers (0.2 to 5μM, up to 60 min, data not shown). Therefore cultures were pretreated with control and MG#1 IgG and human complement for 2 days. Calcium imaging was performed in regions with similar amounts of muscle fibers and dense innervation (Figure 4K, L). The light-induced calcium peaks, when quantified in all fibers identifiable in the visual field, were significantly weaker in cultures treated with MG#1 IgG and complement (n=11) as compared to controls (n=6, Figure 4M, CTRL vs. MG, two-tailed unpaired t test, $p = 0.012$, $t = 2.83$). After application of PYR, we detected a small but

significant increase in the light-induced calcium spike (n=8, Figure 4M, MG vs. MG+PYR, two-tailed paired t test, $p = 0.046$, $t = 2.42$). In addition, the percentage of reactive fibers was reduced in cultures treated with MG#1 IgG and complement compared to controls (Figure 4N, CTRL 78% vs. MG 32%, two-tailed unpaired t test, $p < 0.001$, $t = 4.79$). After application of PYR, we found a tendency towards a higher percentage of fibers displaying a calcium spike, which did not reach significance (Figure 4N, MG vs. MG+PYR, two-tailed paired t test, $p = 0.065$, $t = 2.19$). Finally we sought to confirm the complement attack on the neuromuscular junction. For this purpose, cultures treated with MG#1 IgG and human complement as well as cultures treated with CTRL IgG and human complement for 24h were stained with an antibody recognizing the human complement fragment C3c. Co-labeling with BTX and EYFP revealed targeted complement deposition onto muscle membranes in particular at the neuromuscular junction in MG but not in CTRL cultures. (Figure 4 O, P). Quantification revealed a significantly increased deposition of complement at the neuromuscular junction in in MG cultures as compared to controls (Figure 4 Q, two-tailed unpaired t test, $p = 0.008$, $t = 3.89$). MN-only cultures did not show signs of morphologic deterioration or toxicity (LDH release) when incubated with increasing amounts of MG and control IgG and complement (data not shown).

DISCUSSION

Most anticipated applications of human spinal motorneurons in regenerative medicine (Davis-Dusenbery et al., 2014; Steinbeck and Studer, 2015) depend on their ability to functionally connect to skeletal muscle through neuromuscular junctions. However, the prospect of neuronal graft-to-host connectivity remains insufficiently validated due to technical limitations and the lack of suitable in vitro assays. Using optogenetics, we demonstrate that a human pluripotent stem cell-derived neuronal population with great therapeutic potential functionally connects to its bona fide human target tissue. Our experiments translate the findings of Bryson et al. (Bryson et al., 2014) into a human system. In addition, our in vitro approach allows for an in depth functional characterization of neuromuscular connectivity and the clear exclusion of cell fusion in functional experiments. In our system neuromuscular synaptogenesis likely involves the secretion of agrin by MN terminals which signals through MuSK and rapsyn to induce the assembly of the neuromuscular junction (Sanes and Lichtman, 2001; Wu et al., 2010). The plaque-like AChR clustering (Marques et al., 2000), lack of expression of the adult AChR epsilon subunit and the stimulation-induced enhancement of contractility (Figure 4J) suggest the formation of fully functional, fetal-like neuromuscular synapses. Future refinements of the system could therefore include chronic stimulation paradigms to induce full maturation as well as the addition of other neuronal populations to form multi-synaptic circuits (e.g. spinal interneurons (Maury et al., 2015), cortical neurons (Espuny-Camacho et al., 2013) or Schwann cells (Lee et al., 2010)). The physical separation of muscle and MN cell bodies, 3D scaffolds to organize muscle orientation or matching of the positional identities of MNs and muscle (Philippidou and Dasen, 2013) seem worthwhile as well.

Beyond implications for human regenerative medicine, our novel culture system enables the modeling of neuromuscular disease in an all-human system. In our proof of concept study we show that some of the disease-specific functional and structural phenotypes of the

prototypic neuromuscular disease myasthenia gravis and its treatment (Gold et al., 2008; Verschuuren et al., 2013) can be recapitulated by the simple addition of myasthenia patient IgG and complement. Similar strategies could be employed to investigate rare genetic forms of myasthenia. Our findings indicate that both degenerative as well as regenerative aspects of neuromuscular disease can be studied in this human functional neuromuscular co-culture. Accordingly, we propose that the novel system may enable the dissection of disease processes originating from either side of the neuromuscular junction using patient specific iPSC derived neurons (Kiskinis et al., 2014) or muscle (Darabi et al., 2012; Skoglund et al., 2014).

EXPERIMENTAL PROCEDURES

For extended versions of all experimental procedures see supplemental online material.

Synapsin-hChR2-EYFP hESC line and differentiation into spinal motorneurons

H9 hESCs were stably transduced with lentiviral particles (pLenti-*Syn-hChR2(H134R)-EYFP-WPRE*. Neural induction by dual SMAD inhibition was followed by MN fate specification (Calder et al., 2015). MN clusters were purified by sedimentation.

Human primary myoblast culture and neuromuscular co-cultures

Adult and fetal myoblasts were grown in SkGM-2 medium (Lonza). Differentiation was induced at 70% confluence in medium containing 2% horse serum. Purified MN clusters were resuspended in matrigel and plated on myocultures in MN medium + 2% horse serum.

Co-culture testing, calcium imaging and electrophysiology

Regions with contracting fibers were imaged at room temperature followed by optogenetic stimulation at indicated frequencies and movements were quantified (MetaMorph Software). Myotubes or co-cultures were incubated with Fura-2 and imaged under continuous perfusion. Myotubes were stimulated with acetylcholine (50μM). Co-cultures were illuminated for optogenetic stimulation. Whole-cell current clamp recordings were performed on MNs at room temperature. Light-evoked APs were elicited using a 447 nm diode laser (OEM Laser). Myotubes contracting in response to light were impaled with sharp glass microelectrode for intracellular recordings.

Treatment with human serum and Myasthenia gravis IgG

Serum (containing complement) from 5 healthy donors was pooled and added to the media where indicated (2%v/v). IgG fractions were obtained from 2 severely affected MG patients. Sandoglobulin^{R}, a polyvalent IgG for therapeutic use served as control. Patients had given written consent to use their materials for research and this was approved by the Würzburg University Medical School Ethics Committee.

Immunocytochemistry and imaging

Cells or cultures were fixed in PFA and blocked with 5% FBS/0.3% Triton. Primary antibodies were incubated (Supplementary Table 2) followed by Alexa Flour-conjugated

secondaries. Cells were imaged on inverted fluorescence or confocal microscope followed by data deconvolution.

Supplementary Material

Refer to Web version on PubMed Central for supplementary material.

ACKNOWLEDGMENTS

We thank Sanghoon Oh, Vitaly Boyoko, Sho Fujisawa and Katia Manova (MSKCC molecular cytology core) as well as M. Tomishima (SKI stem cell core) for excellent technical support. K.V.T is the recipient of a senior professorship award funded by the University Medical School, Würzburg. J.A.S. was supported by a DFG fellowship (STE 2064/1-1). The work was supported in part by NIH/NINDS grant NS052671, NYSTEM contract C028503 to L.S. and P30 CA008748.

REFERENCES

Amoroso MW, Croft GF, Williams DJ, O'Keeffe S, Carrasco MA, Davis AR, Roybon L, Oakley DH, Maniatis T, Henderson CE, et al. Accelerated high-yield generation of limb-innervating motor neurons from human stem cells. J Neurosci. 2013; 33:574–586. [PubMed: 23303937]

Barker AT, Jalinous R, Freeston IL. Non-invasive magnetic stimulation of human motor cortex. Lancet. 1985; 1:1106–1107. [PubMed: 2860322]

Boyden ES, Zhang F, Bamberg E, Nagel G, Deisseroth K. Millisecond-timescale, genetically targeted optical control of neural activity. Nature neuroscience. 2005; 8:1263–1268. [PubMed: 16116447]

Bryson JB, Machado CB, Crossley M, Stevenson D, Bros-Facer V, Burrone J, Greensmith L, Lieberam I. Optical control of muscle function by transplantation of stem cell-derived motor neurons in mice. Science. 2014; 344:94–97. [PubMed: 24700859]

Calder EL, Tchieu J, Steinbeck JA, Tu E, Keros S, Ying SW, Jaiswal MK, Cornacchia D, Goldstein PA, Tabar V, et al. Retinoic Acid-Mediated Regulation of GLI3 Enables Efficient Motoneuron Derivation from Human ESCs in the Absence of Extrinsic SHH Activation. J Neurosci. 2015; 35:11462–11481. [PubMed: 26290227]

Chambers SM, Fasano CA, Papapetrou EP, Tomishima M, Sadelain M, Studer L. Highly efficient neural conversion of human ES and iPS cells by dual inhibition of SMAD signaling. Nature biotechnology. 2009; 27:275–280.

Chan A, Lee DH, Linker R, Mohr A, Toyka KV, Gold R. Rescue therapy with anti-CD20 treatment in neuroimmunologic breakthrough disease. Journal of neurology. 2007; 254:1604–1606. [PubMed: 17713826]

Cisterna BA, Cardozo C, Saez JC. Neuronal involvement in muscular atrophy. Frontiers in cellular neuroscience. 2014; 8:405. [PubMed: 25540609]

Cunningham M, Cho JH, Leung A, Savvidis G, Ahn S, Moon M, Lee PK, Han JJ, Azimi N, Kim KS, et al. hPSC-derived maturing GABAergic interneurons ameliorate seizures and abnormal behavior in epileptic mice. Cell stem cell. 2014; 15:559–573. [PubMed: 25517465]

Darabi R, Arpke RW, Irion S, Dimos JT, Grskovic M, Kyba M, Perlingeiro RC. Human ES- and iPS-derived myogenic progenitors restore DYSTROPHIN and improve contractility upon transplantation in dystrophic mice. Cell stem cell. 2012; 10:610–619. [PubMed: 22560081]

Daube JR, Rubin DI. Needle electromyography. Muscle & nerve. 2009; 39:244–270. [PubMed: 19145648]

Davis-Dusenbery BN, Williams LA, Klim JR, Eggan K. How to make spinal motor neurons. Development. 2014; 141:491–501. [PubMed: 24449832]

Drachman DB, Angus CW, Adams RN, Michelson JD, Hoffman GJ. Myasthenic antibodies cross-link acetylcholine receptors to accelerate degradation. The New England journal of medicine. 1978; 298:1116–1122. [PubMed: 643030]

Espuny-Camacho I, Michelsen KA, Gall D, Linaro D, Hasche A, Bonnefont J, Bali C, Orduz D, Bilheu A, Herpoel A, et al. Pyramidal neurons derived from human pluripotent stem cells integrate efficiently into mouse brain circuits in vivo. Neuron. 2013; 77:440–456. [PubMed: 23395372]

Gold R, Hohlfeld R, Toyka KV. Progress in the treatment of myasthenia gravis. Therapeutic advances in neurological disorders. 2008; 1:36–51. [PubMed: 21180568]

Gouti M, Tsakiridis A, Wymeersch FJ, Huang Y, Kleinjung J, Wilson V, Briscoe J. In vitro generation of neuromesodermal progenitors reveals distinct roles for wnt signalling in the specification of spinal cord and paraxial mesoderm identity. PLoS biology. 2014; 12:e1001937. [PubMed: 25157815]

Kiskinis E, Sandoe J, Williams LA, Boulting GL, Moccia R, Wainger BJ, Han S, Peng T, Thams S, Mikkilineni S, et al. Pathways disrupted in human ALS motor neurons identified through genetic correction of mutant SOD1. Cell stem cell. 2014; 14:781–795. [PubMed: 24704492]

Kuwabara S, Yuki N. Axonal Guillain-Barre syndrome: concepts and controversies. The Lancet. Neurology. 2013; 12:1180–1188. [PubMed: 24229616]

Lancaster MA, Knoblich JA. Organogenesis in a dish: modeling development and disease using organoid technologies. Science. 2014; 345:1247125. [PubMed: 25035496]

Lee G, Chambers SM, Tomishima MJ, Studer L. Derivation of neural crest cells from human pluripotent stem cells. Nature protocols. 2010; 5:688–701. [PubMed: 20360764]

Marques MJ, Conchello JA, Lichtman JW. From plaque to pretzel: fold formation and acetylcholine receptor loss at the developing neuromuscular junction. J Neurosci. 2000; 20:3663–3675. [PubMed: 10804208]

Maury Y, Come J, Piskorowski RA, Salah-Mohellibi N, Chevaleyre V, Peschanski M, Martinat C, Nedelec S. Combinatorial analysis of developmental cues efficiently converts human pluripotent stem cells into multiple neuronal subtypes. Nature biotechnology. 2015; 33:89–96.

Mercuri E, Muntoni F. Muscular dystrophies. Lancet. 2013; 381:845–860. [PubMed: 23465426]

Moloney EB, de Winter F, Verhaagen J. ALS as a distal axonopathy: molecular mechanisms affecting neuromuscular junction stability in the presymptomatic stages of the disease. Frontiers in neuroscience. 2014; 8:252. [PubMed: 25177267]

Philippidou P, Dasen JS. Hox genes: choreographers in neural development, architects of circuit organization. Neuron. 2013; 80:12–34. [PubMed: 24094100]

Plomp JJ, Morsch M, Phillips WD, Verschuuren JJ. Electrophysiological analysis of neuromuscular synaptic function in myasthenia gravis patients and animal models. Experimental neurology. 2015

Sahashi K, Engel AG, Lambert EH, Howard FM Jr. Ultrastructural localization of the terminal and lytic ninth complement component (C9) at the motor end-plate in myasthenia gravis. Journal of neuropathology and experimental neurology. 1980; 39:160–172. [PubMed: 7373347]

Sanes JR, Lichtman JW. Induction, assembly, maturation and maintenance of a postsynaptic apparatus. Nature reviews. Neuroscience. 2001; 2:791–805. [PubMed: 11715056]

Sendtner M. Motoneuron disease. Handbook of experimental pharmacology. 2014; 220:411–441. [PubMed: 24668481]

Silva NA, Sousa N, Reis RL, Salgado AJ. From basics to clinical: a comprehensive review on spinal cord injury. Progress in neurobiology. 2014; 114:25–57. [PubMed: 24269804]

Skoglund G, Laine J, Darabi R, Fournier E, Perlingeiro R, Tabti N. Physiological and ultrastructural features of human induced pluripotent and embryonic stem cell-derived skeletal myocytes in vitro. Proceedings of the National Academy of Sciences of the United States of America. 2014; 111:8275–8280. [PubMed: 24843168]

Steinbeck JA, Choi SJ, Mrejeru A, Ganat Y, Deisseroth K, Sulzer D, Mosharov EV, Studer L. Optogenetics enables functional analysis of human embryonic stem cell-derived grafts in a Parkinson's disease model. Nature biotechnology. 2015; 33:204–209.

Steinbeck JA, Studer L. Moving Stem Cells to the Clinic: Potential and Limitations for Brain Repair. Neuron. 2015; 86:187–206. [PubMed: 25856494]

Titulaer MJ, Lang B, Verschuuren JJ. Lambert-Eaton myasthenic syndrome: from clinical characteristics to therapeutic strategies. The Lancet. Neurology. 2011; 10:1098–1107. [PubMed: 22094130]

Toyka KV, Drachman DB, Griffin DE, Pestronk A, Winkelstein JA, Fishbeck KH, Kao I. Myasthenia gravis. Study of humoral immune mechanisms by passive transfer to mice. The New England journal of medicine. 1977; 296:125–131. [PubMed: 831074]

Verschuuren JJ, Huijbers MG, Plomp JJ, Niks EH, Molenaar PC, Martinez-Martinez P, Gomez AM, De Baets MH, Losen M. Pathophysiology of myasthenia gravis with antibodies to the acetylcholine receptor, muscle-specific kinase and low-density lipoprotein receptor-related protein 4. Autoimmunity reviews. 2013; 12:918–923. [PubMed: 23535160]

Wu H, Xiong WC, Mei L. To build a synapse: signaling pathways in neuromuscular junction assembly. Development. 2010; 137:1017–1033. [PubMed: 20215342]

Zhang F, Vierock J, Yizhar O, Fenno LE, Tsunoda S, Kianianmomeni A, Prigge M, Berndt A, Cushman J, Polle J, et al. The microbial opsin family of optogenetic tools. Cell. 2011; 147:1446–1457. [PubMed: 22196724]

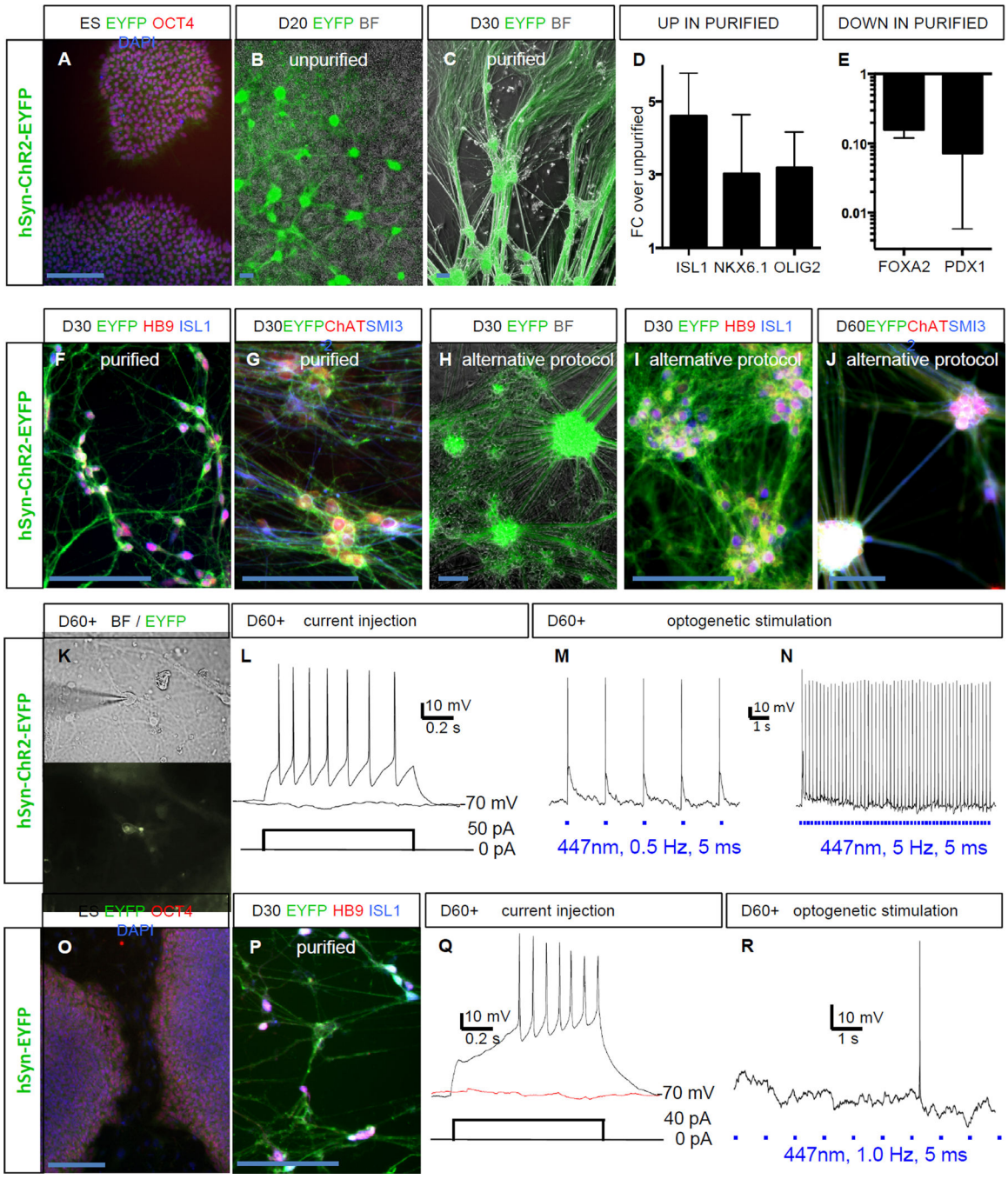

Figure 1. Optogenetic control in hPSC derived spinal motorneurons (MNs)

(A) Clonal hESC line carrying the hSyn-ChR2-EYFP transgene staining for OCT4 (*POU5F1*) and DAPI.

(B) At day 20 (D20) MN clusters express ChR2-EYFP, bright field (BF).

(C) After purification MN clusters are enriched.

(D) qRT-PCR, after purification sMN markers are up-regulated.

(E) qRT-PCR, after purification non-neuronal markers are down-regulated.

(F) At day 30 spinal MNs express ChR2-EYFP and stain for HB9 and ISL1.

(G) At day 30 spinal MNs co-stain for ChAT and SMI32.
(H) Alternative protocol ChR2-EYFP+ MNs.
(I) At day 30 spinal MNs (alternative protocol) express ChR2-EYFP, HB9 and ISL1.
(J) At day 60 spinal MNs (alternative protocol) express ChR2-EYFP, ChAT and SMI32.
(K) Neuron in bright field and EYFP channel chosen for electrophysiology.
(L) Beyond day 60 (D60+) hESC-derived MNs fire action potentials in response to depolarizing current injection.
(M, N) Mature ChR2+ hESC-derived MNs faithfully fire action potentials in response to optogenetic stimulation.
(O) Clonal hESC line carrying the hSyn-EYFP transgene staining for OCT4 and DAPI.
(P) At day 30 purified spinal hESC-derived MNs express EYFP, HB9 and ISL1.
(Q) Mature EYFP+ hESC-derived MN fires action potentials in response to current injection.
(R) Mature EYFP+ hESC-derived MNs do not respond to light stimulation.
Scale bars 100 μM. Error bars represent SEM.

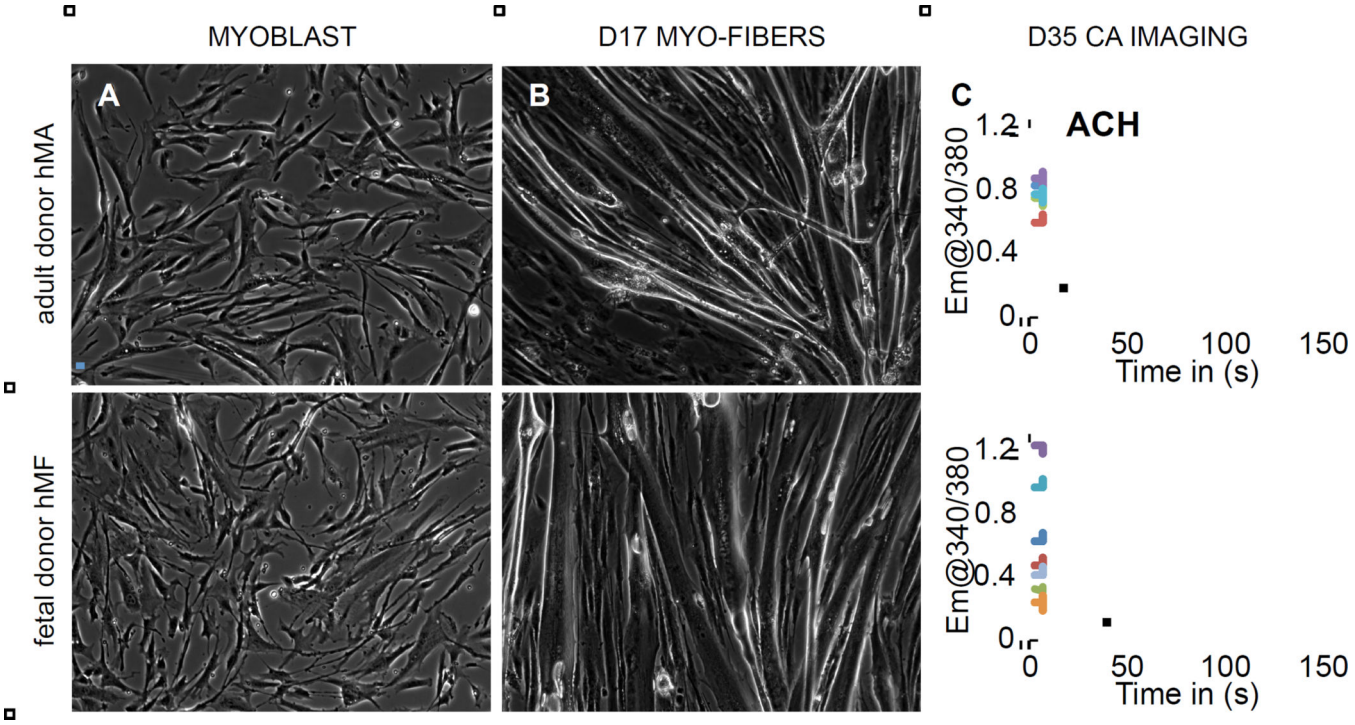

Figure 2. Generation of functional human myofibers

(A) Human myoblasts derived from an adult donor (hMA, upper panel) and a fetal donor (hMF, lower panel).

(B) Human myofibers at day 17 of differentiation.

(C) Calcium imaging in human myofibers on day 35. Acetylcholine (ACh) induces a robust calcium transient. Each trace resembles a distinct fiber.

Scale bars 100 μM.

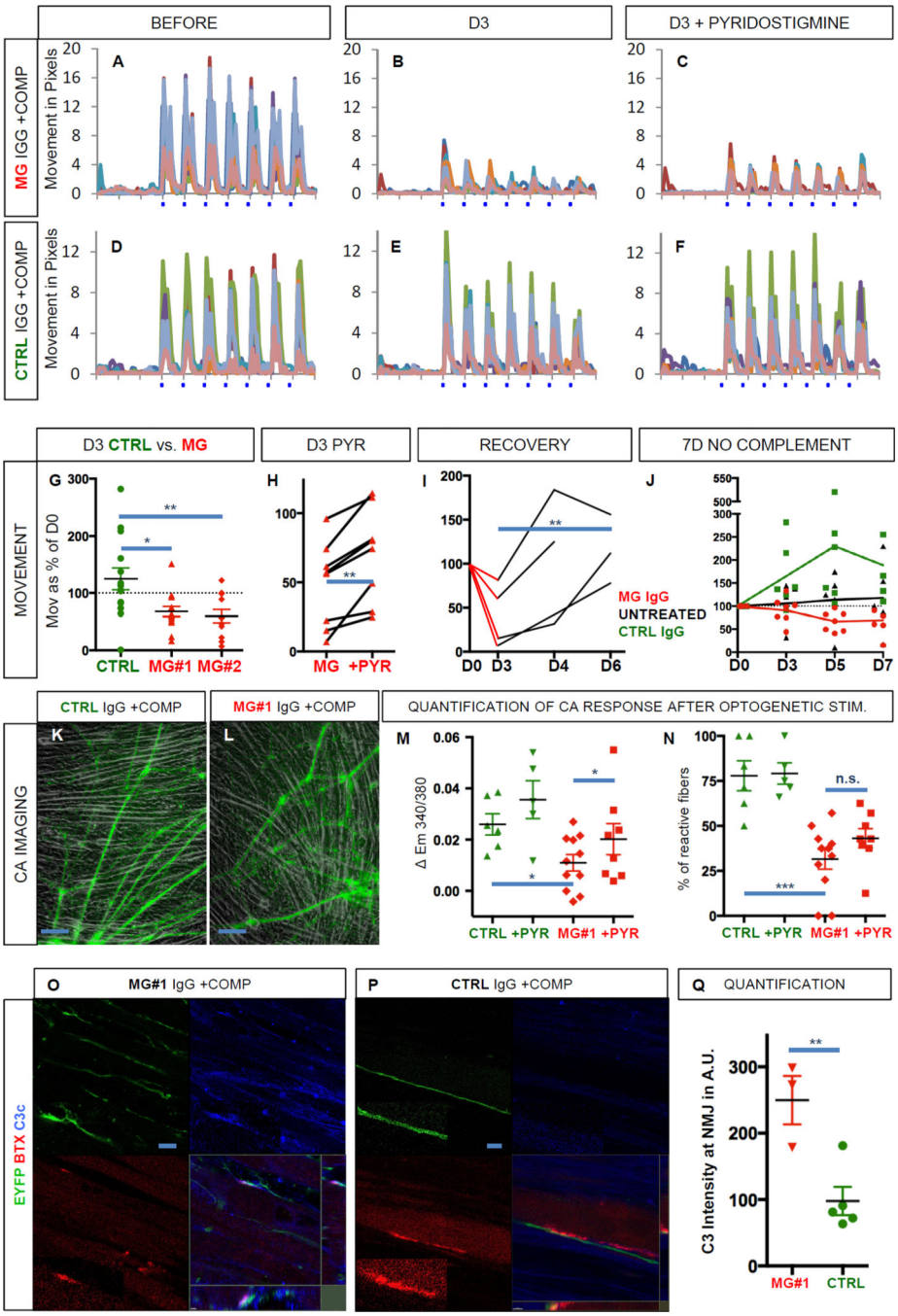

Figure 3. Characterization of neuromuscular co-cultures

(A, E) Co-cultures of spinal hESC-derived MNs with adult (hMA) and fetal (hMF) derived myofibers 1 week (1W) after initiation, EYFP and bright field channels.

(B, F) Co-cultures of spinal hESC-derived MNs with adult (hMA) and fetal (hMF) derived myofibers 6–8 weeks after initiation. (Online version of Fig. 3 containing videos).

(C, G) Quantification of muscle twitches in co-cultures in response to optogenetic stimulation for 50s (upper panel) and 500s (lower panel). Each trace resembles a distinct fiber.

(D, H) Vecuronium (2μM) blocks light-evoked contractility in adult (D) and fetal (H) myofibers.
(I) EYFP and bright field picture of calcium imaging experiment shown in J.
(J) Ratiometric analysis of calcium transients in myofibers in response to optogenetic stimulation for 2 min (upper panel) and 40 min (lower panel). Each trace resembles a distinct fiber.
(K) Sharp microelectrode recording from a single myofiber. Generation of vecuronium-sensitive action potentials in response to optogenetic stimulation at 0.2 and 2 Hz.
(L) Long-term stability of neuromuscular connectivity. Movement in individual regions was quantified on day 5, 15 and 25 and compared to movement on day 0, normalized at 100%.
(M) Co-cultures contain a layer of vimentin+ and GFAP+ stroma.
(N) Co-cultures show dense network of EYFP+ axons and desmin+ muscle fibers.
(O) Multinucleated and striated myofiber in close contact with EYFP+ neuronal processes in contractile region.
(P) High-power confocal imaging of clustered acetylcholine receptor (BTX) in close association with EYFP+ neuronal process and synaptophysin labeling.
(Q, R) Contracting regions (CONTR, left) and non-contracting regions (NO CONTR, right) were compared for AChR clustering. Quantification of BTX+ dots revealed a significant increase in contracting / innervated regions. * $p < 0.05$.
In C, D and G, H one pixel corresponds to 0.5 μm. Scale bars 100μm, except I, K 50 μm and P, Q 25 μm.

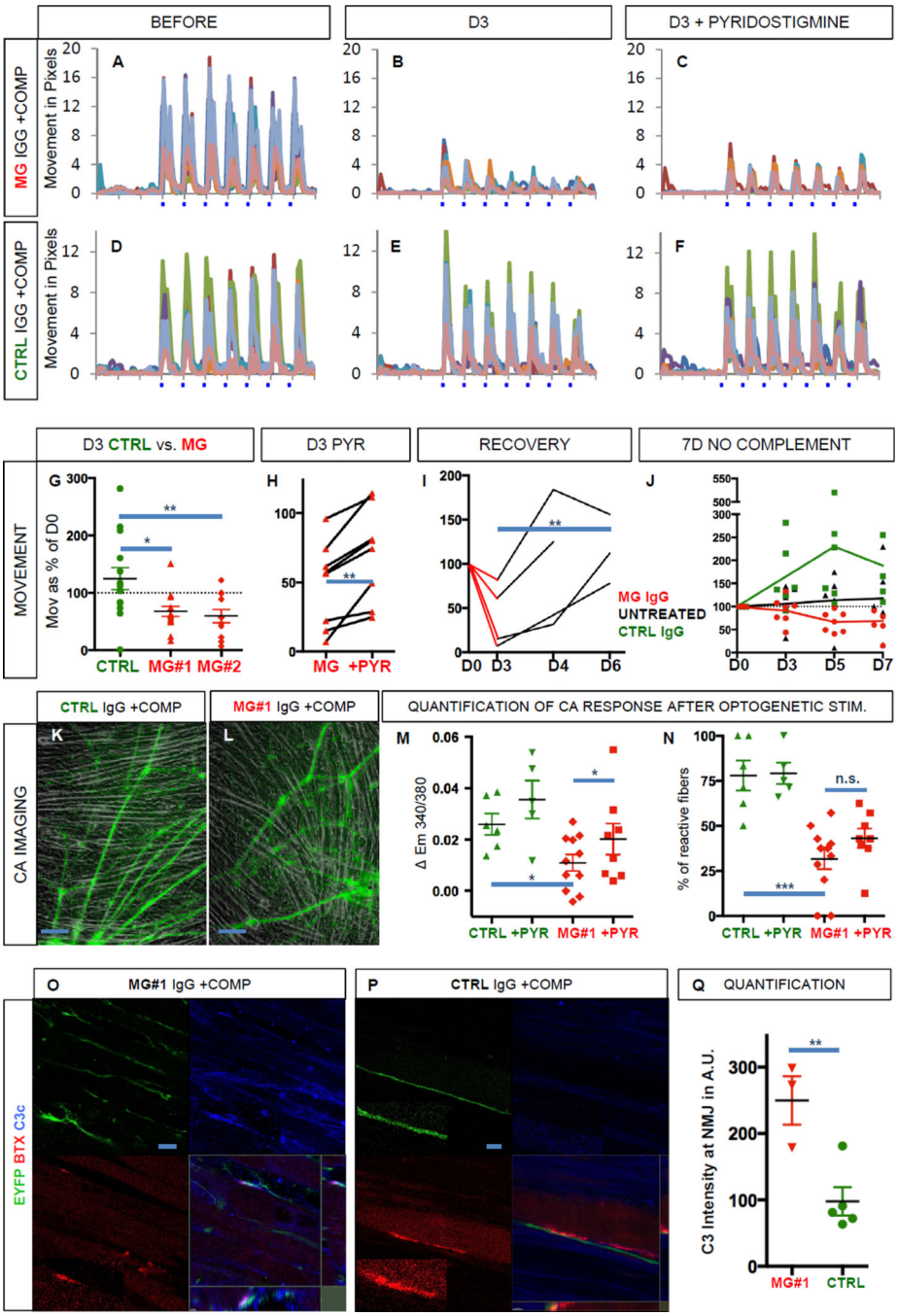

Figure 4. Modeling of neuromuscular transmission failure, typical of Myasthenia gravis

(A, D) Kinetogram of mature, contracting co-cultures of spinal MNs with adult myofibers (hMA) before the addition of myasthenia gravis (MG) IgG (patient 2) and complement (A) or control IgG and complement (D).

(B, E) Same co-cultures as in A and D, on day 3 after the addition of myasthenia gravis IgG and complement (B) or control IgG and complement (E).

(C, F) Same co-cultures as in B and E after the addition of pyridostigmine (PYR, 10 μM) on day 3.

(G) Quantification of movement in cultures treated with MG IgG (patient #1 and 2) and complement or control IgG and complement on day 3 in % as compared to day 0.
(H) Quantification of movement in cultures treated with MG IgG (patient #1 & 2 combined) and complement before and after the addition of pyridostigmine on day 3.
(I) Recovery of movement on day 4 and day 6 after wash out of MG IgG (patient #1 & 2 combined) and complement on day 3.
(J) Quantification of movement in cultures treated with MG IgG (patient #1), control IgG and in untreated cultures, all without complement.
(K, L) Bright field and EYFP images of functional MN co-cultures with adult muscle (hMA) treated with MG IgG (patient #1) and complement or control IgG and complement at 48h in regions selected for calcium imaging.
(M) Quantification of the calcium increase in response to optogenetic stimulation in MG and control cultures and after the addition of PYR.
(N) Percentage of reactive fibers in response to optogenetic stimulation in MG and control cultures and after the addition of PYR.
(O, P, Q) Immunocytochemistry and quantification (Q) for the deposition of the human complement component C3c (blue) onto the neuromuscular junction co-labeled for EYFP (green) and BTX (red) 24h after the addition of MG IgG (patient #1) or control IgG and complement. Area in small boxes with dotted line are magnified in boxes with solid line. Scale bars 100 μm in K, L; 10 μm in O, P. In A–F one pixel corresponds to 0.5 μm. n.s. = not significant, * $p < 0.05$, ** $p < 0.01$, *** $p < 0.001$. All error bars represent SEM.